A novel approach to high temperature solar receivers with an absorbing gas as heat transfer fluid and reduced radiative losses

Gianluca Ambrosetti*, Philipp Good

Synhelion SA, Via Cantonale 19, 6900 Lugano, Switzerland

ABSTRACT

We report on a new high temperature solar receiver concept which exploits the ability of some molecular gases such as water vapor or carbon dioxide to absorb a significant fraction of longer wavelength thermal radiation while being mostly transparent to terrestrial solar radiation. The receiver operation principle is similar to the "greenhouse effect": It relies on a gas volume between an aperture and a black surface heated by solar radiation to absorb the thermal re-radiation of the surface and shield the aperture from it. At the same time, the gas is heated by such absorption and acts as heat transfer fluid (HTF). The receiver works with radiation only as heat transfer mechanism and does not require, *a priori*, any convective contribution. To demonstrate the potential of the approach we modelled the system with the most accurate method available, spectral line-by-line (LBL) photon Monte Carlo raytracing with the absorption coefficients derived from the HITEMP 2010 spectroscopic database. We applied the model to a cylindrical cavity geometry with an axial gas flow. We simulated the performance for a large 16 m diameter, 16 m-long near-ambient pressure receiver with and without window at the 100 m^2-aperture. The gases considered as HTF were steam, CO_2, and mixtures of them. The gas outlet temperature was varied between 1000 K and 2000 K. We also simulated a small 1.6 m diameter, 1.6 m-long cylindrical cavity receiver with a 1 m^2 windowed aperture and pressurized steam at 10 bar. With a solar irradiation flux of 1200 kW/m^2 at the aperture, the receiver efficiency remained above 80% for gas outlet temperatures up to 1800 K for all receivers operated with steam. Carbon dioxide led to lower efficiencies, but water-rich mixtures of H_2O and CO_2 performed closely as good as pure steam. The proposed receiver concept represents a new opportunity towards low-cost high temperature solar technologies for processes beyond 1000 K.

1. Introduction

High temperature processes account for a large share of the world energy requirements. One third of the overall industrial energy consumption is used for heating processes at above 700 K (IEA-ESTAP and IRENA, 2015), with processes above 1300 K being dominant (Naegler et al., 2015). One third of the world primary energy consumption is used for fossil fuel-fired thermal power generation (IEA, 2016). Steam and combined cycle power plants all involve combustion temperatures well above 1300 K and steam temperatures in excess of 870 K. Concentrated solar systems have the potential to reach among the highest temperatures required by man-made processes. Solar furnaces can easily reach temperatures in excess of 3000 K (Winston et al., 2005). However, high specific costs and practical constraints on attainable conversion efficiencies have hampered the widespread use of such installations and confined their application to research facilities. Still, lower temperature systems have attained industrial-scale deployment,

especially concentrated solar power (CSP) installations for power generation. State of the art CSP plants operate nowadays at temperatures just below 870 K. The quest for viable high temperature technologies above 870 K is an active field of research (Hoffschmidt, 2014; Ho and Iverson, 2014). With the experience gained from large scale central receiver (tower) power plants (Romero-Alvarez and Zarza, 2007), economically sustainable high concentration tower systems are at hand. North field layouts can achieve average irradiation fluxes of $1200 - 1500$ kW/m^2 without secondary concentrators. This is enough for operation at 1300 K and above (Romero-Alvarez and Zarza, 2007). However, choosing an appropriate heat transfer fluid (HTF) and devising a solar receiver architecture able to exchange efficiently with the fluid remains challenging.

Among the possible choices for high temperature HTFs, gaseous fluids have been extensively investigated, in particular air (Ávila-Marín, 2011; Ho and Iverson, 2014; Good et al., 2015, 2016). Pressurized CO_2 has also been considered (Turchi, 2009; Ho and Iverson, 2014; Caliot

---

Nomenclature

Latin characters

Bo	Boltzmann number, $Bo = k\kappa_P/(4\sigma T^3)$
c_p	specific heat, J/(kg K)
$D_{aperture}$	receiver aperture diameter, m
D_{cavity}	receiver cavity diameter, m
E_η	solar spectral irradiance, W/m^2 cm
H	receiver cavity height, m
h	enthalpy, J/kg
k	thermal conductivity, W/(m K)
L	path length, m
$\dot{m}$	mass flow rate, kg/s
N_r	cavity radial segment number
n_r	cavity radial segment index
N_z	cavity axial segment number
n_z	cavity axial segment index
p	gas partial pressure, bar
$\mathbf{q}_{rad}$	radiative heat flux vector, W/m^2
Q	power (or energy flux), MW
q	heat flux (density), kW/m^2
$Q_{absorbed}$	power removed by the gas, MW
Q_{solar}	solar power incident on receiver aperture, MW
q_{solar}	solar flux incident on receiver aperture, kW/m^2
Q_{losses}	receiver losses, MW
r	radial coordinate, m
T	temperature, K
T_g	gas temperature, K
T_{in}	gas inlet temperature, K
T_{out}	gas outlet temperature, K
u_r	radial velocity component, m/s

u_z	axial velocity component, m/s
$u_{z,in}$	gas inlet velocity, m/s
z	axial coordinate, m

Greek characters

α_{solar}	total absorptivity of solar radiation
ϵ_η	spectral emissivity
ϵ_s	surface emissivity
η	efficiency; wavenumber, cm^{-1} (Appendix A)
η_{rec}	receiver efficiency, $\eta_{rec} = Q_{absorbed}/Q_{solar}$
κ_P	Planck mean absorption coefficient, 1/m
ρ	density, kg/m^3
ρ_{in}	gas inlet density, kg/m^3
σ	Stefan-Boltzmann constant, $\sigma = 5.67 \cdot 10^{-8}\, W/(m^2\, K^4)$

Subscripts and superscripts

g	gas
j	general index
rec	receiver
s	surface
η	spectral (wavenumber)

Abbreviations

AM	air mass
CSP	concentrated solar power
DNI	direct normal irradiance, W/m^2
HITEMP	high-temperature molecular spectroscopic database
HTF	heat transfer fluid
LBL	line-by-line

and Flamant, 2014; Khivsara et al., 2016). The superheating sections in direct steam generation plants also deal with a gaseous HTF. Advantages of gaseous HTFs include no relevant operating temperature limit, no high-temperature phase change, low or no HTF costs, no toxicity, and possibility of direct use with a Brayton cycle (pressurized air and supercritical CO_2) (Turchi, 2009; Good et al, 2015). Disadvantages include low density and low thermal conductivity. By far the most successful approach to gas receiver designs is the volumetric absorber concept, chiefly applied to air systems (Ávila-Marín, 2011). Still, volumetric receivers suffer from shortcomings such as energy losses associated with the air return ratio (in open-loop volumetric receivers), flow instability, absorber material durability, and absorber cost (Ávila-Marín, 2011; Ho and Iverson, 2014).

We propose an alternative path towards reduced re-emission, high efficiency, and reduced costs with a gas receiver concept which exploits the ability of polyatomic gases such as water vapor and CO_2 to absorb significantly in the infrared spectrum while being transparent to most of the terrestrial solar spectrum. The receiver system does not require, in principle, any convective contribution to the heat transfer, allowing for the elimination of the expensive and challenging absorber-heat exchanger element.

We report on the receiver concept, modelling, validation, and simulation. The aim of the present work is more to illustrate and substantiate the potential of the proposed approach than the identification of optimal designs and the performance estimation of practical embodiments. Therefore, while we carry out an in-depth analysis of the radiative heat transfer mechanisms in the system, we limit ourselves to a simple cylindrical cavity geometry and a simplified fluid flow. We analyze the impact on performance of the relevant parameters such as HTF composition, pressure, inlet and outlet temperature, solar irradiation flux, and effect of aperture window.

2. The receiver concept

Asymmetric diatomic gases such as CO or NO as well as polyatomic gases such as H_2O, CO_2, NH_3 or CH_4 have important absorption bands in the wavelength range of thermal radiation (Hottel and Sarofim, 1967; Edwards, 1981; Siegel and Howell, 1992; Modest, 2013). If we consider the total emissivities of these gases (see e.g. the charts for steam[1] and CO_2 of Refs. (Hottel and Sarofim, 1967; Leckner, 1972; Alberti et al., 2015; Alberti et al., 2016)) it becomes apparent that sufficiently large gas volumes, in the order of several meters, have the potential to absorb a significant fraction of the thermal radiation emitted by hot surfaces. Both large volumes and high temperature surfaces are found in cavity central receivers for large north fields, suggesting a possible heat transfer mechanism for a solar receiver. This reasoning, together with the observation that participating gases of practical interest such as steam and CO_2 are mostly transparent to the terrestrial solar spectrum, form the basis of the receiver concept of the present work.

The receiver is constituted by an absorbing cavity with a windowed aperture. The cavity is filled with the streaming gas flowing from the aperture towards the back of the cavity. The incoming solar radiation enters the aperture, passes with minimal absorption through the gas, and is successively absorbed by a highly absorptive surface at the back of the cavity. The solar-absorbing surface thermalizes and re-radiates with a blackbody spectrum. The gas absorbs to a large extent the thermal re-emission and is heated up, and, at the same time, shields the aperture from this re-emission. Fig. 1 shows a schematic illustration of the concept.

---

[1] In the following of the present work we consider steam and water vapor to be the same and use the expressions as synonyms.
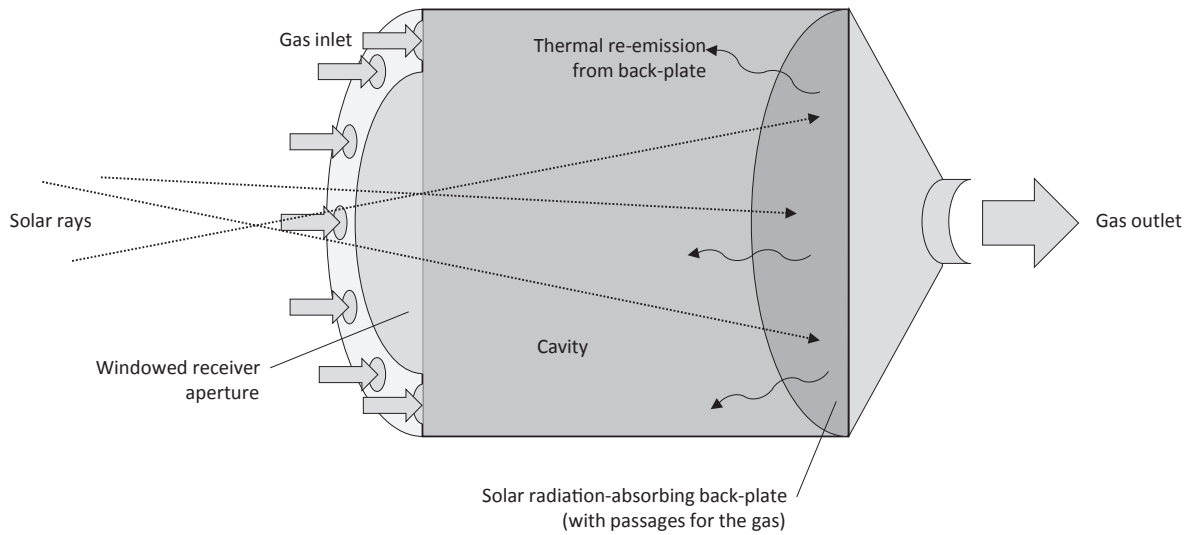
Fig. 1. Schematic illustration of the absorbing gas receiver concept.

In principle the receiver could work with radiation only as exchange mechanism (i.e. no forced convection). When the absorbing gas HTF is at ambient pressure the cavity must be comparably large for the gas to absorb a significant amount of radiation. To give an idea, the total absorptivity of an isothermal gas at 1400 K to radiation from a black-body at 2000 K along a path length of 16 m is 0.65 for water vapor and 0.22 for CO_2. As the following sections will show, a cavity receiver of such dimensions operating with the proposed approach can achieve very high solar-to-thermal conversion efficiencies: With steam, efficiencies close to 90% can be expected at outlet temperatures as high as 1400 K, and efficiencies close to 80% can be maintained even at an outlet temperature of 2000 K. With CO_2, an efficiency of 60% is still attainable at an operating temperature of 1400 K. Furthermore, the participating gas pressure can be used to reduce system size: in fact, the size of the cavity can be reduced by a factor equivalent to the pressure increase without compromising performance.

Despite the similarities with the "greenhouse effect" (Siegel and Howell, 1992; Modest, 2013) routinely exploited in glazed solar collectors, and with the well-known atmospheric phenomenon with the same name, the use of the above concept in combination with molecular participating gases for high temperature solar receivers is, to our knowledge, unreported. Solar receivers with participating media have been investigated nonetheless with externally-irradiated tubular configurations with the HTF flowing inside the duct for supercritical CO_2 (Caliot and Flamant, 2014; Khivsara et al., 2016). However, these receivers are substantially different from the approach introduced in the present work as the HTF is never on the same side of the irradiated surface and, therefore, cannot shield an aperture from the re-emission of the surface. A further difference to these works is that they relied by design on an important convective fraction of the overall heat transfer to the fluid.

3. Receiver modeling

For the purposes of the present work we model the receiver as a 2D axisymmetric cylindrical cavity (see Fig. 2). The gas flow is modelled as inviscid as described by Euler's momentum equation. No buoyancy effect is included. A purely axial, uniform velocity profile (plug flow) is set at the inlet (aperture) plane,

$$u_{z,\text{in}} = \frac{4\dot{m}}{\rho_{\text{in}} \pi D_{\text{cavity}}^2}$$

where $\dot{m}$ is the mass flow rate and ρ_{in} the density at the inlet temperature T_{in}. Since $u_{z,\text{in}}$ is typically in the order of 1 m/s and the

pressure drop due to acceleration of the fluid across the receiver is below 1 Pa, a uniform pressure is applied to the whole domain. Accordingly, the radial velocity component remains zero in the whole receiver,

$$u_r = 0$$

The continuity equation then simplifies to

$$\frac{\partial}{\partial z}(\rho u_z) = 0$$

At the operating conditions considered in the present work, radiation is the dominant heat transfer mechanism and conduction in the gas as well as convection from the walls are neglected. To substantiate this, we may consider that the conduction-to-radiation parameter defined as $k\kappa_P/(4\sigma T^3)$ (Modest, 2013) (where k is the thermal conductivity and κ_P the Planck mean absorption coefficient of the gas) evaluated at a typical temperature of 1400 K and pressure of 1 bar is in the order of 10^{-3} for water vapor and CO_2. Similarly, the convection-to-radiation parameter or Boltzmann number $Bo = \rho c_p u_z/(4\sigma T^3)$ (Modest, 2013) (with c_p the isobaric specific heat) is typically below 10^{-2} under most operating conditions. Accordingly, the energy conservation equation in terms of enthalpy h may be written as

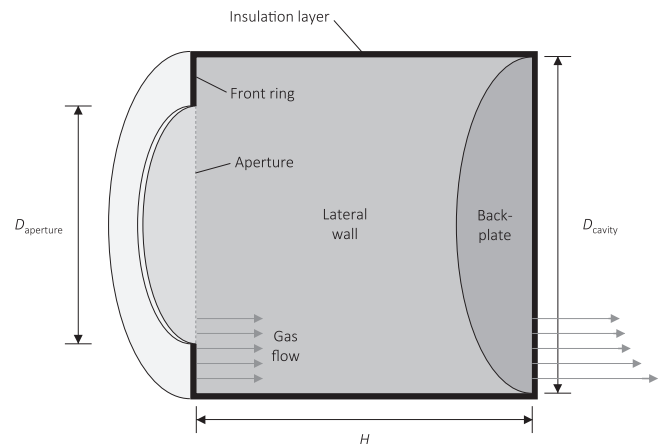$$\frac{\partial}{\partial z}(\rho u_z h) = \nabla \cdot \mathbf{q}_{\text{rad}}$$

Fig. 2. Cylindrical cavity receiver model. The inlet gas flow extends to the entire aperture and front ring plane. The outlet gas flow extends to the entire back plate plane.

where $\nabla \cdot \mathbf{q}_{rad}$ is the divergence of the radiative heat flux vector which acts as volumetric heat source. Thermal radiation exchange is modeled with Monte Carlo raytracing (standard photon Monte Carlo method (Modest, 1992, 2013; Wang and Modest, 2007)), which is the closest approach to the underlying physical mechanisms of the exchange. Photon bundles (rays) of a single wavenumber are traced from their point of emission to their point of absorption. Scattering is neglected because the gas is considered free of soot and other particles and scattering by gas molecules is negligible in heat transfer applications (Modest, 2013). The raytracing procedure is based on the mocacyl_std.f code available as supplementary material to Ref. (Modest, 2013) with modifications to fit our needs as described in the following. The location of emission from the gas is determined using random number relations calculated for the gas temperature field (Modest, 2013). For emission wavenumber, line-by-line (LBL) spectral random number relations are generated according to the methodology of (Wang and Modest, 2007) for H_2O, CO_2, and $H_2O - CO_2$ mixtures from the respective spectral and temperature-dependent absorption coefficients obtained from the HITEMP 2010 spectroscopic database (Rothman et al., 2010). The linear absorption coefficients are generated with the procedures described in (Kangwanpongpan et al., 2012; Alberti et al., 2015, 2016) in a code derived from the fskdist.f90 routine available as supplementary material to (Modest, 2013). The sub-Lorentzian behavior of the lineshapes is handled with the cutoff approach of (Alberti et al., 2015, 2016). The random number relationships are calculated prior to raytracing using a modified version of the rnarray.f code provided with Ref. (Modest, 2013). Although computationally intensive, the LBL method retains the most complete information of the spectral properties of the gases (Wang and Modest, 2007).

The surfaces of the cavity are assumed to emit diffusely with a blackbody spectrum. Surfaces are black ($\epsilon_s = 1$). The receiver enclosure is considered to be perfectly insulated (adiabatic walls) and conduction in the solid walls is neglected. For the aperture we consider a windowless case, as it could be with e.g. a gas curtain (Flesch et al., 2016) and the case of a windowed aperture composed of a fused silica window. For the open case the aperture is a black surface with fixed uniform temperature of 300 K. The window is taken as a 10 mm-thick single flat sheet, although a realistic large window will be sectioned, and a pressurized design will require a dome shape to withstand the load (Hertel et al., 2016). Spectral and directional selectivity of the window are taken into account. Similarly to the participating gas, the location, wavenumber and direction of emission from the window are sampled from random number relationships calculated according to (Modest, 2013) prior to raytracing for the temperature distribution on the window. The spectral, directional absorptance, reflectance and transmittance of the window are calculated from the refractive and absorptive indices as predicted by electromagnetic theory (Modest, 2013) using spectral properties of fused silica from (Philipp, 1998). Reflection from the window is assumed as specular. Heat losses through the windowed aperture occur by transmission of thermal re-radiation from the gas and cavity walls and thermal emission from the window to the surroundings. Absorption, reflection and transmission of concentrated solar irradiation is evaluated separately once for all by weighting the corresponding spectral, directional properties with the ASTM G173-03 reference spectrum for direct normal irradiance (DNI) at an air mass of 1.5 (AM 1.5) (ASTM, 2012) and the incidence angle distribution on the window resulting from a 45° rim angle paraboloidal source, respectively. The resulting solar and directionally weighted absorptance, reflectance and transmittance are 0.003, 0.073 and 0.924, respectively, and the latter figure is used to adjust accordingly the solar power entering the windowed receivers. No other heat transfer mechanism (e.g. free or forced convection) is considered for the window.

The contribution of direct absorption of solar radiation within the gas, in the order of a few percent (see Appendix A), is neglected. Concentrated solar radiation is assumed to be fully absorbed on the cavity surfaces, and radiation is assumed to be impinging on the back-plate only. The flux distribution on the back-plate is taken as uniform. The discretization procedure of the cavity surfaces and volume is described in Appendix B.

Turning to the numerical solution procedure, the gas inlet temperature T_{in}, gas outlet temperature T_{out}, and an initial estimate of the temperature field of the gas and walls are given as input parameters. The program then determines the unknown surface and volume element temperatures as well as the total gas mass flow by iterative solving of the energy conservation equation for all gas volumes and surface segments. To reduce statistical noise and computational times, a time-blending (or tempered averaging) scheme (Feldick and Modest, 2012; Modest, 2013) is used to find a first solution. In this approach, at each iteration the thermal radiative exchange simulated by Monte Carlo raytracing with a reduced number of rays ($\sim 10^7$) is blended with the results from the previous iterations and the temperatures are adjusted accordingly. The time-blending solution is refined further by increasing the number of rays to $2 \cdot 10^9$ and adjusting the temperature field based on the simulated thermal radiative exchange of the last iteration only using a relaxation factor in the range of 0.5 for convergence purposes of the nonlinear problem (Patankar, 1980). The final solution is then averaged over several iterations such that the overall energy conservation is satisfied to below 0.01% of the solar power incident on the receiver's aperture.

4. Results

To illustrate quantitatively the potential of the receiver concept presented here we have chosen two cylindrical cavity receiver designs: (i) a large design with a cavity diameter $D_{cavity} = 15.96$ m (for a 200 m² back-plate area), a cavity height $H = D_{cavity}$, and a receiver aperture diameter $D_{aperture} = 11.28$ m (for an aperture area of 100 m²), and (ii) a small design with a cavity diameter $D_{cavity} = 1.596$ m (for a 2 m² back-plate area), a cavity height $H = D_{cavity}$, and a receiver aperture diameter $D_{aperture} = 1.128$ m (for an aperture area of 1 m²), i.e. with all dimensions rescaled to 1/10th of the large case. The large receiver is considered with the gases at near-ambient pressure (1 bar), while the small receiver is considered with the gases under pressure at 10 bar. Two versions, one with and one without aperture window, are evaluated for the large design, while the small design, being pressurized, is always windowed. The average solar irradiation flux is considered for the base case as 1200 kW/m² on the aperture area, spreading out over the back-plate at 600 kW/m² for the windowless aperture, consistent with what it would be with a high concentration solar field. For the windowed aperture the solar irradiation flux on the back-plate is reduced by 7.6% to 554.4 kW/m² to take into account the reflection and absorption losses at the window. The absorption coefficients used for the LBL Monte Carlo simulation of the participating gases span the wavenumber range 1–29,000 cm^{-1} for water vapor, 5–12,785 cm^{-1} for CO_2, and 1–29,000 cm^{-1} for $H_2O - CO_2$ mixtures. The wavenumber resolution is 0.01 cm^{-1}. The temperature range is 400–2500 K, with a resolution of 100 K. Values for wavenumbers and temperatures in between are calculated during simulation by bilinear interpolation.

Regarding the gas flow, for the base cases the HTF streams in the axial direction along the receiver axis as described at the beginning of Section 3. These cases are denoted in the results as "axial flow". We also compute sometimes a conservative case where the whole gas volume within the receiver is at uniform temperature T_g equal to the outlet temperature T_{out}. Following (Hottel and Sarofim, 1967) we denote this
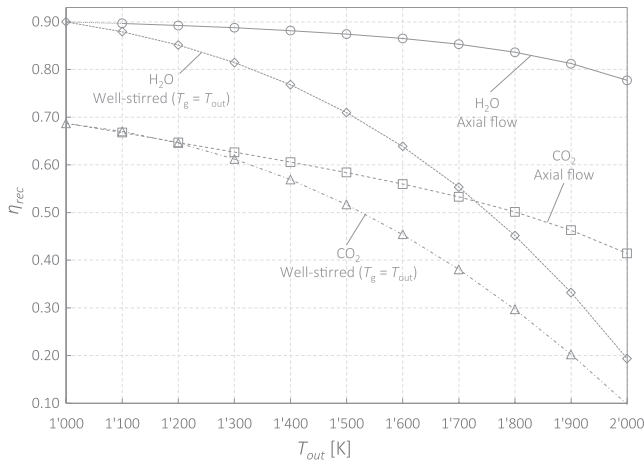
Fig. 3. Windowless large receiver with H_2O vapor and CO_2 at 1 bar and gas inlet temperature $T_{in} = 1000$ K. Receiver efficiency as a function of T_{out} for the axial flow and well stirred ($T_g = T_{out}$) cases.

case as "well-stirred" or $T_g = T_{out}$. For practical purposes this can be taken as the most conservative performance estimate.

4.1. Validation

We first performed a verification of the absorption coefficients generated for the LBL calculation by computing the total emissivities of water vapor, CO_2 and H_2O – CO_2 mixtures by numerical integration. The agreement with the results of Refs. (Alberti et al., 2015, 2016) was excellent. Agreement with the results of Kangwanpongpan et al. (2012) was also very good, although a slight tendency to lower emissivity values at lower temperatures was observed (in the order of 2–3%), possibly due to the inclusion in our case of the lineshape cutoff of (Alberti et al., 2015, 2016).

We then used our code for simulating the radiative heat transfer from an emitting and absorbing, cylindrical gas volume at a total pressure of 1 bar to its base and lateral surface boundaries as described in Wang and Modest (2007). In the first case, the gas is at a uniform temperature of 1620 K and contains 1.4% of CO_2 and 2.8% of H_2O vapor (molar fractions). In the second case, a hot cylindrical core at 1600 K with 10% CO_2 and 5% H_2O vapor is surrounded by a cold annular layer at 500 K containing 5% CO_2 and 10% H_2O vapor (Wang and Modest, 2007). The agreement of surface wall heat fluxes on the base and lateral wall segments given in Wang and Modest (2007) and simulated with our code was within 3% and 6% for the uniform and step case, respectively. The difference is mainly attributed to the older spectroscopic databases used in Wang and Modest (2007) (HITEMP 2000 for H_2O, CDSD 1000 for CO_2) compared to HITEMP 2010 used in this work, which contains more absorption lines (Rothman et al., 2010) and generally yields slightly higher wall heat fluxes.

We finally performed a comparison of the LBL Monte Carlo results with the predictions of the net radiation method (Hottel and Sarofim, 1967; Siegel and Howell, 1992). We considered the large windowless receiver with water vapor at uniform temperature. The surfaces (back-plate, lateral wall, and front ring) are not discretized and have a uniform temperature. For the gas total emissivity, we used the values of Alberti et al. (2016). The outcomes were nearly identical, with the relative differences between the receiver efficiency results of the LBL model and the ones of the net radiation method remaining below 0.5% in the 1000–1800 K water vapor temperature range.

4.2. Performance of different gas types

We consider first how the receiver performance is influenced by the absorbing gas composition. In the range of operating conditions of the

present work, water vapor has the highest total emissivity figures among the possible practical choices of participating gases (see e.g. (Hottel and Sarofim, 1967; Leckner, 1972; Alberti et al., 2016)). The other realistic choice is carbon dioxide (Alberti et al., 2015). However, CO_2 absorbs almost 3 times less than water vapor under the conditions of interest. Fig. 3 shows the receiver efficiency for the large windowless receiver with steam and CO_2 at 1 bar as a function of the outlet temperature for an inlet temperature of 1000 K. The receiver efficiency is defined as

$$\eta_{rec} = Q_{absorbed}/Q_{solar}$$

with $Q_{absorbed}$ the total power removed by the gas and Q_{solar} the total solar power incident on the receiver aperture. For water vapor and axial flow, η_{rec} remains above 80% for most of the outlet temperatures, underlining the performance potential of the concept. Even the conservative well-stirred cases offer decent performances up to 1700 K. On the other side, CO_2 shows lower efficiencies, making its use alone impractical. Still, mixtures of H_2O vapor and CO_2 have much better total emissivity figures, especially when water-rich (Kangwangpongpan et al., 2012). Therefore, we simulated the receiver performance for different H_2O – CO_2 mixtures again for the large windowless receiver at 1 bar and T_{in} of 1000 K. Fig. 4 reports the receiver efficiency as a function of the H_2O molar fraction at two different T_{out}. It emerges that, besides for low water contents, efficiency remains relatively unaffected by a reduced water molar fraction. This is of relevance, since H_2O – CO_2 HTFs are interesting for integration with oxy-fuel combustion systems: In principle, the solar circuit could operate directly with the (filtered) flue gases without the requirement of any heat exchanger. For the rest of this work we will consider water vapor only.

4.3. Temperature profiles of the receiver surfaces and gas volume

We ascribe the high performances of the receiver concept to two main mechanisms, which we want to analyze further in this section and in the following Section 4.4. The first mechanism is the capacity of the gas to shield the aperture from the thermal emission of the back-plate and the lateral walls. This is directly linked to the absorptivity of the gas and its capacity of being heated by such emission. To give an idea, the total transmissivity of steam at 1 bar and 1400 K to blackbody radiation at 2000 K over a path length of 16 m is 0.35. However, in the proposed design the cavity effect reduces further the transmitted fraction. Radiation emitted from the back-plate and hitting the (adiabatic) front ring and lateral wall is re-emitted with a new blackbody spectrum according to the local wall temperature. Again, part of this radiation is absorbed by the gas, transmitted to the aperture, and transmitted to the
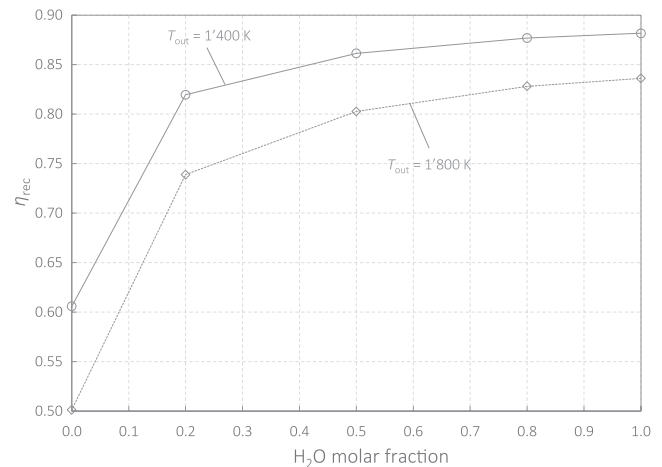

Fig. 4. Windowless large receiver. Receiver efficiency as a function of the water molar fraction in H_2O – CO_2 mixtures at 1 bar total pressure and $T_{in} = 1000$ K for the axial flow cases $T_{out} = 1400$ K and $T_{out} = 1800$ K.
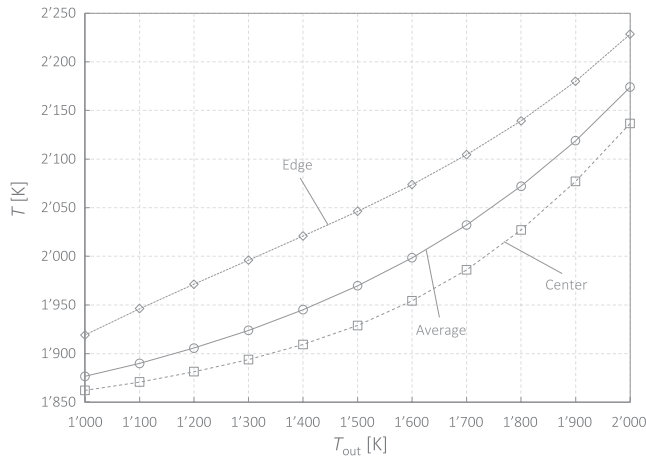
Fig. 5. Windowless large receiver with H_2O vapor at 1 bar and T_{in} = 1000 K. Center (minimum), average, and edge (maximum) back-plate temperatures as a function of T_{out} (The 1000 K data points are for the well-stirred case).

cavity walls. Eventually, for the T_{in} = 1000 K – T_{out} = 1400 K case only around 8.2% of the net thermal radiative heat flux leaving the back-plate (= solar power reaching the back-plate) reaches the aperture, of which 3.5% comes from the back-plate directly, and 4.7% from the lateral wall, see Fig. 10 and Section 4.6. Fig. 5 shows the back-plate average surface temperature as well as its temperatures at the center and at the edge (adjacent the lateral wall) for different receiver outlet temperatures. The back-plate temperature distribution is quite uniform,

as it is expected with the uniform solar flux distribution we assume. It is interesting to observe that the back-plate temperatures raise only weakly as the gas outlet temperature increases, with the temperature difference between back-plate and gas outlet dropping from around 900 K at T_{out} = 1000 K to around 200 K at T_{out} = 2000 K.

The second mechanism is the build-up of an axial temperature gradient which confines the hotter (radiating) gas layers to the back of the cavity and produces a further self-shielding effect. This is a consequence of the axial flow of the gas. The gas volume temperature profiles for the 1400 K and 1800 K outlet temperature cases are shown in Fig. 6 as contour plots and in Fig. 7 as radial average. In both figures the axial temperature gradient is well visible. To assess the impact of the axial temperature gradient we can go back to Fig. 3 and compare the axial flow results with the well-stirred results. The well-stirred cases have the whole gas volume at the outlet temperature and by construction have no temperature gradient. Considering again the case of T_{out} = 1400 K, losses through the aperture by thermal emission from the gas amounts to 13.4% of the solar power input in the well-stirred case, while in the case of axial flow with T_{in} = 1000 K they reduce to 3.6% (see Fig. 10 and Section 4.6). Therefore, a successful practical embodiment of the concept should strive to achieve an axial flow. This can be challenging in practice when a design needs to operate at low gas velocities, e.g. at reduced solar irradiance conditions or when operating under pressure. In addition, when large temperature gains between T_{in} and T_{out} need to be achieved, buoyancy might strongly affect the flow and cause axial recirculation in a horizontal receiver, whereas in a downward facing central receiver it might contribute to the formation of a temperature gradient.
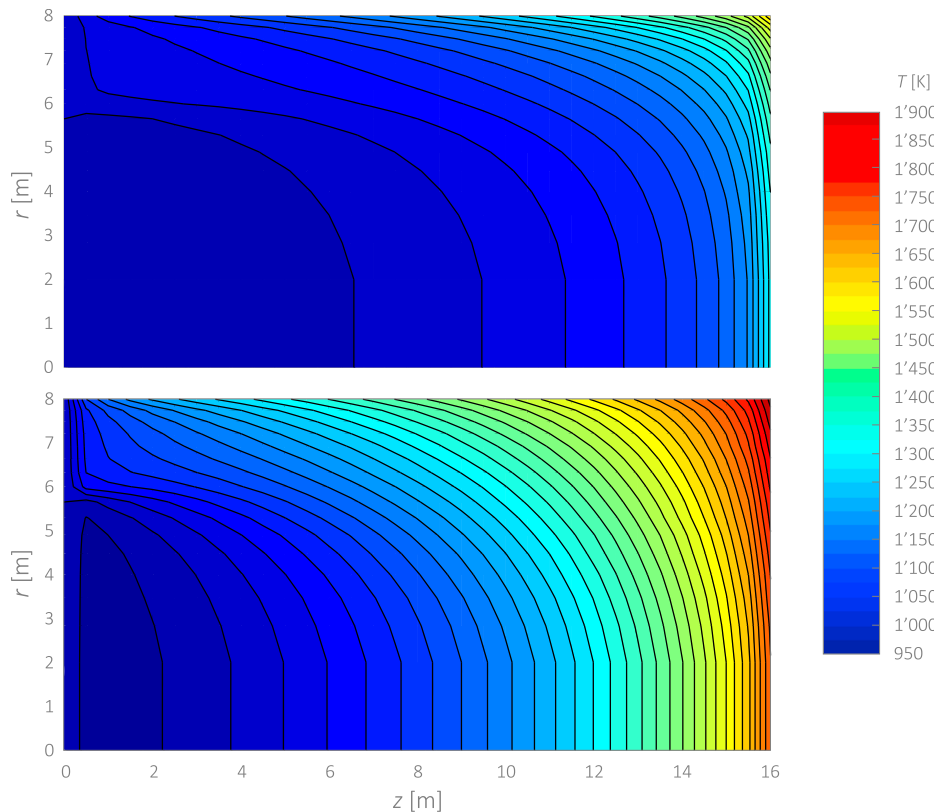

Fig. 6. Windowless large receiver with H_2O vapor at 1 bar and T_{in} = 1000 K with axial flow. Gas temperature contour plots in the longitudinal cross section plane for the T_{out} = 1400 K (top) and T_{out} = 1800 K (bottom) cases.
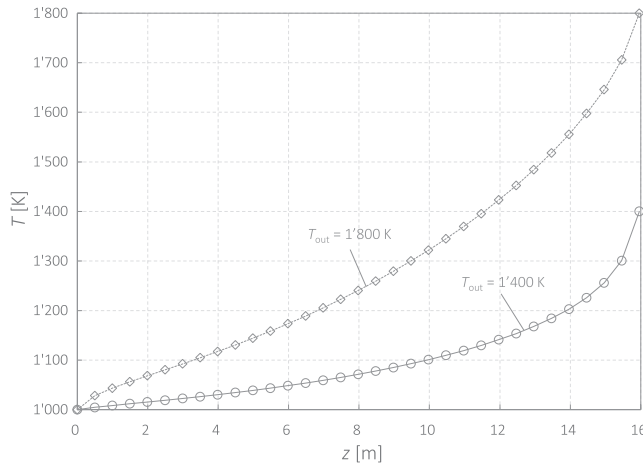
Fig. 7. Windowless large receiver with H_2O vapor at 1 bar and $T_{in} = 1000$ K for the $T_{out} = 1400$ K and $T_{out} = 1800$ K axial flow cases. Radial-averaged axial gas temperature profiles.
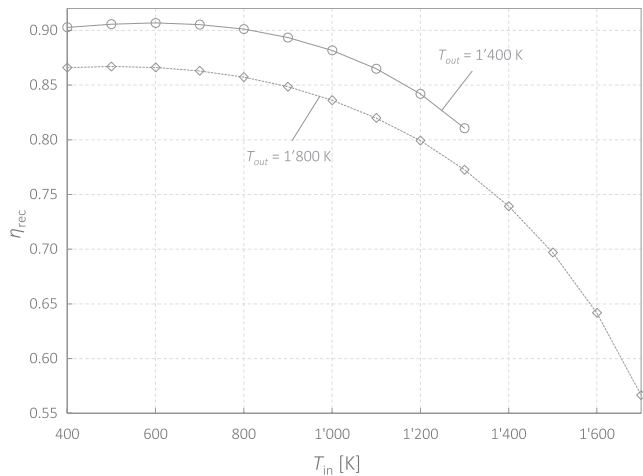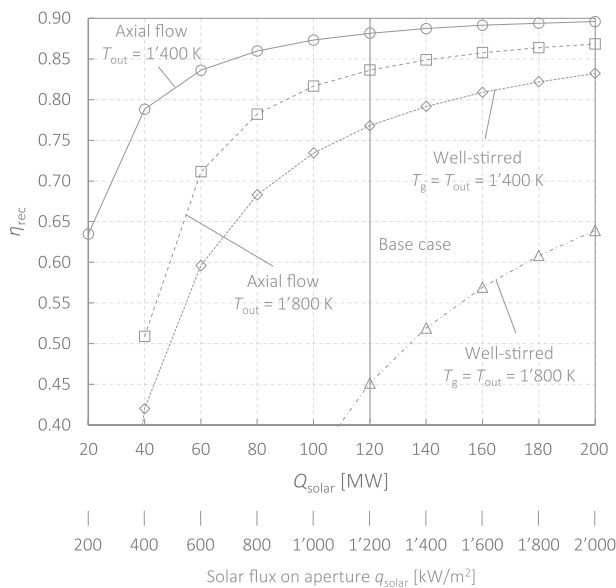

Fig. 8. Windowless large receiver with H_2O vapor at 1 bar. Receiver efficiency as a function of T_{in} for the $T_{out} = 1400$ K and $T_{out} = 1800$ K axial flow cases.

4.4. Inlet temperature

The effect of the axial temperature gradient and of having the colder gas layers close to the aperture can be further assessed by considering the system efficiency as a function of the inlet temperature for a fixed T_{out}. Fig. 8 shows that for the 1400 K and 1800 K outlet temperature axial flow cases. The efficiency drops more markedly as $T_{out} - T_{in}$ gets smaller, consistently with the progressive reduction of the axial temperature gradient effect. It also appears that the behavior at lower temperatures is non-monotonic, with a maximum around $T_{in} = 600$ K. We attribute this effect to the drop in the emissivity of water vapor for large path lengths at temperatures below 800 K (see e.g. (Alberti et al., 2016)).

4.5. Input power (solar flux)

A central aspect of a receiver design is its performance at partial load, when the solar flux entering the aperture is reduced. It is also useful to see how higher concentrations can improve efficiency. Fig. 9 displays η_{rec} (left) and the total power lost through the aperture (right) for different solar power inputs for the axial flow ($T_{in} = 1000$ K) and well stirred cases with $T_{out} = 1400$ K and $T_{out} = 1800$ K. All cases show a similar trend in the total losses through the aperture, with a near-linear regime and similar slopes. This indicates that, in this regime, the heat loss variation at different solar power inputs is correlated more with the shielding effect of the gas than with the axial temperature gradient and is due principally to the fact that the transmitted fraction of emission from the back-plate and lateral wall becomes smaller (larger) at lower (higher) input powers. This is because the back-plate achieves the blackbody emission at lower (higher) temperatures to which the gas is more (less) absorbing. Still, at lower input powers the axial temperature gradient build-up gets also weaker and eventually breaks down. This is behind the trend deviation at $T_{out} = 1800$ K and $Q_{solar} < 100$ MW.

4.6. Cavity size

The large cavity dimensions of the near-ambient pressure receiver were chosen to be compatible with its application on a large high concentration north field. Yet, smaller systems may be of practical
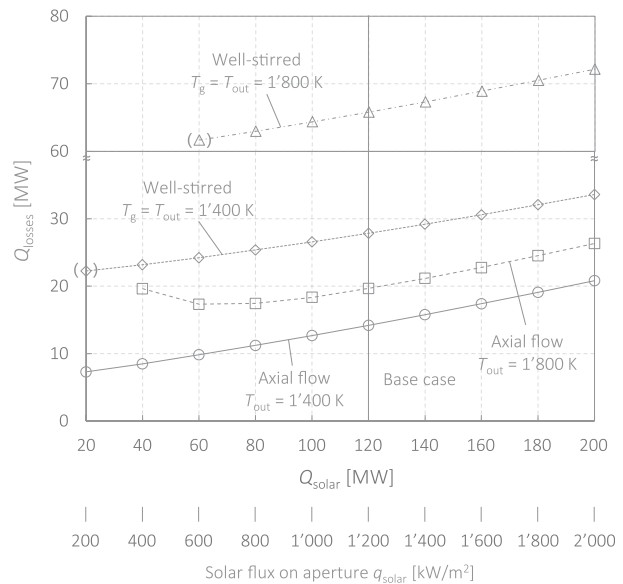

Fig. 9. Windowless large receiver with H_2O vapor at 1 bar and $T_{in} = 1000$ K for the cases $T_{out} = 1400$ K, $T_{out} = 1800$ K, and the well-stirred cases $T_g = T_{out} = 1400$ K and $T_g = T_{out} = 1800$ K. (Left) Receiver efficiency as a function of the solar input power (excerpt). (Right) Total power lost through the aperture $Q_{losses} = Q_{solar} - Q_{absorbed}$ as a function of the solar input power. The lowest power results for the well-stirred cases are in parentheses because they entail a negative efficiency.
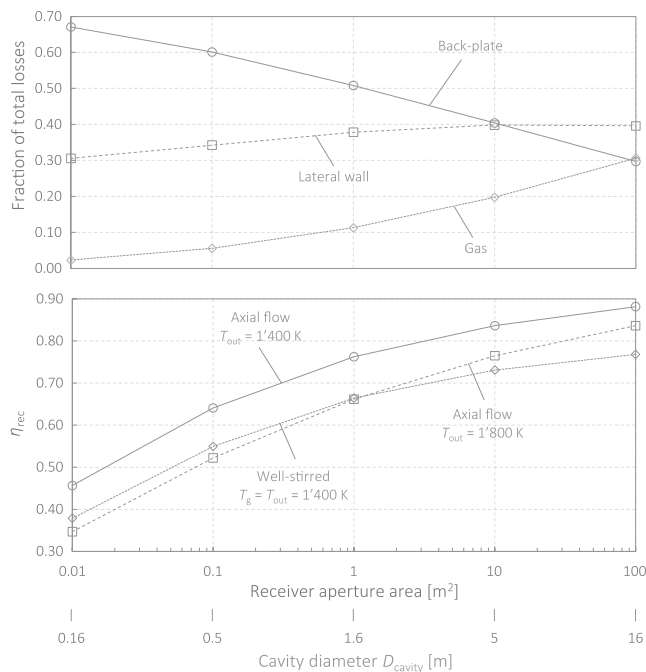
Fig. 10. Windowless receivers with H_2O vapor at 1 bar and $T_{in} = 1000$ K. (Top) Breakdown of losses by thermal emission from the back-plate, lateral wall and gas volume for axial flow and $T_{out} = 1400$ K. (Bottom) Receiver efficiency as a function of receiver cavity size for the axial flow cases $T_{out} = 1400$ K, $T_{out} = 1800$ K, and the well stirred case $T_g = T_{out} = 1400$ K.

interest as well. Therefore, we investigated the effect of cavity size on the receiver efficiency. The results are reported in the bottom plot of Fig. 10. The aspect ratio (height-to-diameter ratio) of unity was kept for all cases. The solar flux at the receiver aperture was maintained at 1200 kW/m². The figure evidences that there is indeed some flexibility towards smaller designs and that the cavity diameter can be reduced by at least a factor of two without compromising excessively the receiver efficiency. The losses breakdown among the back-plate, lateral wall and gas volume, assessed by binning the rays escaping through the aperture by their point of emission, as a function of receiver size is shown in the top panel of Fig. 10 for the axial flow case with $T_{out} = 1400$ K. As it may be expected, for smaller systems the re-radiation losses from the back-plate and lateral wall are dominant, while for larger cavities, where the shielding effect of the gas becomes more important, thermal emission from the gas itself becomes a main component.

4.7. Receiver aperture with window

The practical construction of a large gas-filled cavity receiver with a windowless aperture is highly challenging and probably not feasible without a certain degree of HTF spillage, as it would be with gas curtains or similar approaches. Accordingly, it is likely that most implementations will require a window closing the aperture. Therefore, we simulated the receiver performance with a fused silica window as described in Section 3. Fig. 11 shows the efficiency as a function of T_{out} for the large receiver with water vapor at 1 bar, $T_{in} = 1000$ K and axial flow. We can observe that the overall receiver efficiency drops with respect to the windowless case. This is to be ascribed to the reflection and absorption losses of incoming solar irradiation (7.6%) at the window and, therefore, the lower power reaching the back-plate. On the other hand, the window reduces re-radiation losses through the aperture, measured in percentage of the solar power reaching the back-
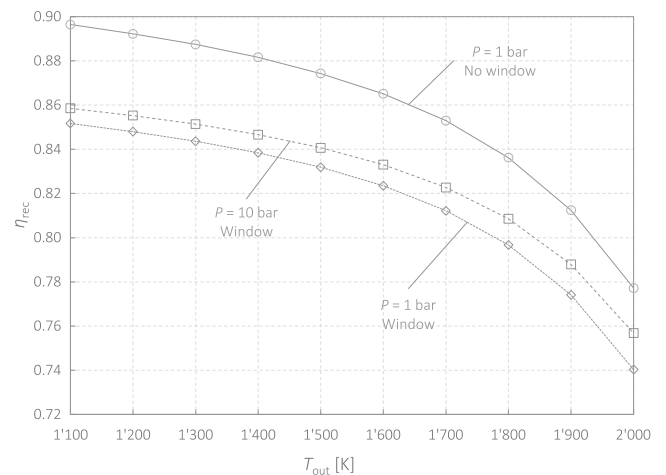

Fig. 11. Windowed large receiver with H_2O vapor at 1 bar and windowed small receiver with H_2O vapor at 10 bar. Receiver efficiency as a function of T_{out} for axial flow and $T_{in} = 1000$ K. Reference results for the windowless large receiver (Fig. 3) are included for comparison.

plate, by about 2.5% with respect to the windowless case at all operating temperatures. The window temperatures were found to be relatively uniform (typically a few degrees between maximum and minimum, raising to 22 K for $T_{out} = 2000$ K) and did not vary significantly with the gas outlet temperature, increasing from an average of 890 K at $T_{out} = 1100$ K to 990 K at $T_{out} = 2000$ K.

4.8. Pressurized receiver

The gas pressure has a strong impact on the total emissivity of a participating species, with higher pressures leading to higher emissivities. This is due in the first order to the higher molecule number per unit volume, and then principally to the effects of collision broadening (Hottel and Sarofim, 1967). Fig. 11 shows the efficiency of the windowed small receiver operated with water vapor at 10 bar and $T_{in} = 1000$ K as a function of T_{out}. Since the number of molecules within the cavity was kept constant with respect to the large receiver at 1 bar, the efficiency increase of the pressurized receiver is due to the latter effect of collision broadening. The pressurized receiver, as all cavity receivers under pressure, is challenging from a construction standpoint because of the pressure-bearing aperture window. However, many applications exist where a pressurized HTF is required by the process to which the solar circuit is interfaced (such as e.g. a Brayton cycle). Furthermore, the size (and power) reduction possibilities that come along may make a pressurized receiver an attractive option also for applications where pressure is not demanded.

5. Conclusion and outlook

A new high temperature solar receiver concept exploiting the ability of some molecular gases to absorb a significant fraction of longer wavelength thermal radiation while being mainly transparent to terrestrial solar radiation has been described. The receiver operation principle is akin to the "greenhouse effect", and relies on radiation only as heat transfer mechanism to heat the gaseous HTF. We verified the effectiveness of the approach by modelling the system with the most accurate method available, spectral LBL photon Monte Carlo raytracing, and with the high-resolution spectral absorption coefficients derived from the most complete high temperature spectroscopic database, HITEMP 2010 (Rothman et al., 2010). We applied the model to a cylindrical cavity geometry with an axial gas flow. We simulated the performance

for a large 16 m diameter, 16 m-long near-ambient pressure receiver with and without window on the aperture with water vapor, CO_2, and mixtures of them as HTF. We simulated as well a small 1.6 m diameter, 1.6 m-long windowed receiver with pressurized steam at 10 bar. With a solar irradiation flux of 1200 kW/m^2 at the aperture, the receiver efficiency remained above 80% for gas outlet temperatures up to 1800 K for all receivers operated with water vapor. Carbon dioxide led to lower performances, but water-rich mixtures of H_2O and CO_2 displayed efficiencies very close to the ones of pure steam. These efficiency figures are highly promising. For comparison, existing state-of-the art pressurized air closed volumetric receivers with a ceramic convective exchanger such as the high temperature unit of the SOLGATE receiver cluster (European Commission, 2005; Heller et al., 2006) can achieve solar-to-thermal efficiencies around 80% with an outlet temperature of 1230 K and a concentrated solar radiation flux at the receiver aperture of around 750 kW/m^2.

The potential of the concept is further reinforced by the remarkably simple architecture of the receiver: In principle, a sufficiently large gas volume between the receiver aperture and the absorbing surface on which the concentrated solar radiation impinges and thermalizes is the only prerequisite for the system to work. The practical design and construction of the receiver implies a few aspects where care is needed. As with many cavity receiver designs, a window or other aperture-shielding solution is required. The surface temperatures of the absorber back-plate can reach temperatures in excess of 2000 K, so adequate refractory materials must be employed. The materials must also withstand the oxidizing character of steam and CO_2. Finally, an important aspect for the optimal exploitation of the concept is the sustain of an axial flow of the gaseous HTF from the aperture side towards the back-plate. A practical embodiment should try to achieve this also at reduced mass flows and when buoyancy effects are present.

Acknowledgments

Appendix A. Direct absorption of solar radiation

We report here the results of the assessment of the direct absorption of terrestrial solar radiation by water vapor and carbon dioxide. Given the spectral irradiance of the sun E_η, the absorptivity of the gas may be calculated as:

$$\alpha_{\text{solar}} = \frac{\int_0^\infty \epsilon_\eta E_\eta \, d\eta}{\int_0^\infty E_\eta \, d\eta}$$

where ϵ_η is the gas spectral emissivity. We calculated the absorptivity by numerical integration with the absorption coefficients generated from the HITEMP 2010 database for the LBL simulation. The terrestrial solar spectrum was taken as the ASTM G173-03 reference spectrum for direct normal irradiance (DNI) at an air mass of 1.5 (AM 1.5) (ASTM, 2012). We report in Fig. A1 α_{solar} for steam and CO_2 for different partial pressure path length products pL as a function of the gas temperature.

It can be appreciated that, if for CO_2 the absorbed fraction is minimal, for water vapor it can easily reach a few percent. Still, in the present work we consider this contribution as negligible, and do not include it in the calculations.
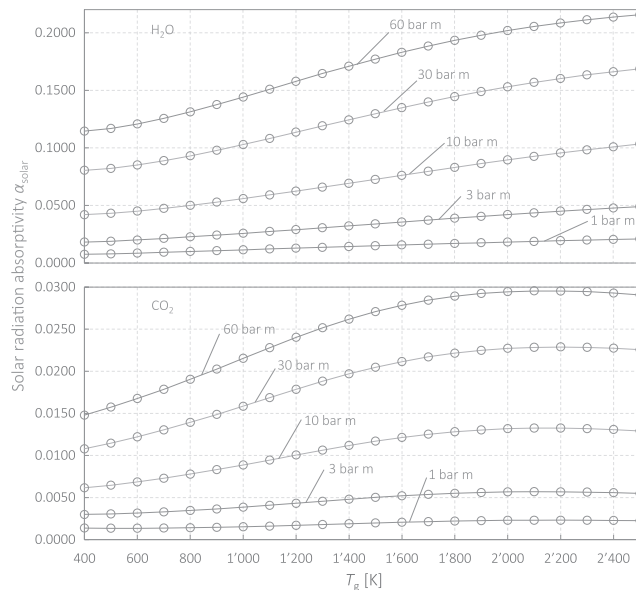

Fig. A1. H_2O vapor (top) and CO_2 (bottom) at a total pressure of 1 bar. Solar radiation absorptivity as a function of gas temperature for different pressure path lengths pL.

Appendix B. Receiver cavity discretization

The cavity surfaces and gas volume are discretized with a 2D axisymmetric sectioning (Fig. B1). Axial segments are all of equal length H/N_z, with N_z the number of axial segments, and are labelled by index n_z. Radial sectioning is performed with concentric cylindrical shells in such a way that the cross-sectional area of each shell is constant and equal to $\pi\,D_{cavity}^2/(4\,N_r)$, with N_r the number of radial shells. Therefore, if n_r is the shell index, the outer radius r_j of shell number $n_r = j$ will be $r_j = (D_{cavity}/2)\sqrt{j/N_r}$. The gas flow is discretized using the upwind scheme (Patankar, 1980), i.e. the gas temperature within each control volume (n_r, n_z) is considered constant and equal to its gas outlet temperature in axial direction entering the downstream volume $(n_r, n_z + 1)$. The heat capacity at constant pressure is evaluated at the gas volume temperatures using 6th-order polynomial fits of the values in the 400–2500 K range given by the CoolProp library (Bell et al., 2014). Stepwise constant temperature profiles are applied as well to the cavity walls and window, which yields a first order accurate numerical method. The upwind scheme (Patankar, 1980) has the advantage that for one single volume it converges to the well-stirred enclosure approximation (Hottel and Sarofim, 1967) where the full gas volume is at the outlet temperature. The well-stirred enclosure can be evaluated effectively with the net radiation method for verification purposes, as done in Section 4.1.

A fixed ratio of 2 is kept between the axial segment number N_z and the radial shells/rings number N_r: $N_z = 2\,N_r$. In this way, the axial segment length and the average of the radial shell thicknesses is the same. In general, an increase of axial segmentation leads to an (initially strong) increase in receiver efficiency. This is due to the temperature gradient that progressively develops as N_z increases and that confines the hotter radiating gas layers further to the back of the cavity. Larger radial shell numbers, on the other side, lead to a slight decrease in receiver efficiency due to the build-up of hotter shells near the lateral wall. The combined increase of N_r and N_z with the fixed ratio $N_z = 2\,N_r$ leads generally to higher efficiencies, with the effect becoming stronger at higher gas outlet temperatures and higher gas inlet to outlet temperature differences. We have chosen a discretization with $N_z = 32$ and $N_r = 16$ which provided a manageable compromise between accuracy and computing time. This level of refinement allows to capture with sufficient detail the main behaviors and trends of the system. However, it entails underestimated efficiencies at the highest temperatures (in the order of 1.5% for water vapor at 1 bar, $T_{in} = 1000$ K and $T_{out} = 2000$ K), which is conservative and considered acceptable in light of the simplified treatment of the fluid of the present work.
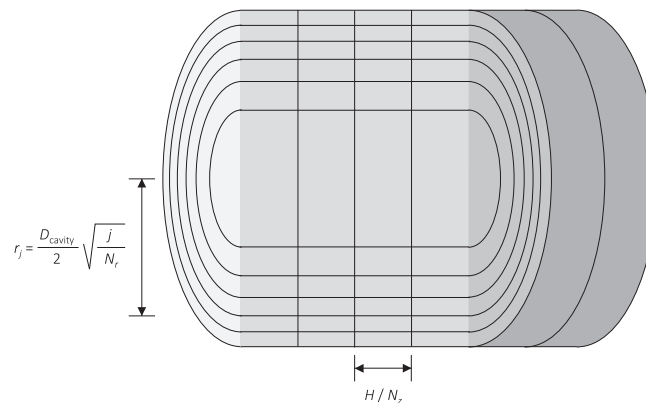

$$r_j = \frac{D_{cavity}}{2}\sqrt{\frac{j}{N_r}}$$

H/N_z

Fig. B1. 2D discretization of cavity surfaces and volume.

References

Alberti, M., Weber, R., Mancini, M., 2015. Re-creating Hottel's emissivity charts for carbon dioxide and extending them to 40 bar pressure using HITEMP-2010 data base. Combust. Flame 162, 597–612.

Alberti, M., Weber, R., Mancini, M., 2016. Re-creating Hottel's emissivity charts for water vapor and extending them to 40 bar pressure using HITEMP-2010 data base. Combust. Flame 169, 141–153.

ASTM G173-03, 2012. Standard tables for reference solar spectral irradiances: Direct normal and hemispherical on 37° tilted surface.

Ávila-Marín, A.L., 2011. Volumetric receivers in solar thermal power plants with central receiver system technology: a review. Sol. Energy 85, 891–910.

Bell, I.H., Wronski, J., Quoilin, S., Lemort, V., 2014. Pure and pseudo-pure fluid thermophysical property evaluation and the open-source thermophysical property library CoolProp. Ind. Eng. Chem. Res. 53, 2498–2508.

Caliot, C., Flamant, G., 2014. Pressurized carbon dioxide as heat transfer fluid: influence of radiation on turbulent flow characteristics in pipe. AIMS Energy 3, 172–182.

Edwards, D.K., 1981. Radiation Heat Transfer Notes. Hemisphere, New York.

European Commission, 2005. SOLGATE - Solar hybrid gas turbine electric power system. Final Project Report, EUR 21615.

Feldick, A.M., Modest, M.F., 2012. A spectrally accurate two-dimensional axisymmetric, tightly coupled photon Monte Carlo radiative transfer equation solver for hypersonic entry flows. J. Heat Transf. 134, 122701.

Flesch, R., Grobbel, J., Stadler, H., Uhlig, R., Hoffschmidt, B., 2016. Reducing the convective losses of cavity receivers. In: Proc. SolarPACES 2015, AIP Conf. Proc. 1734, 030014.

Good, P., Ambrosetti, G., Pedretti, A., Steinfeld, A., 2015. An array of coiled absorber tubes for solar trough concentrators operating with air at 600 °C and above. Sol. Energy 111, 378–395.

Good, P., Ambrosetti, G., Pedretti, A., Steinfeld, A., 2016. A 1.2 MWth solar parabolic trough system based on air as heat transfer fluid at 500 °C — Engineering design,

modelling, construction, and testing. Sol. Energy 139, 398–411.

Heller, H., Pfänder, M., Denk, T., Tellez, F., Valverde, A., Fernandez, J., Ring, A., 2006. Test and evaluation of a solar powered gas turbine system. Sol. Energy 80, 1225–1230.

Hertel, J., Uhlig, R., Söhn, M., Schenk, C., Helsch, G., Bornhöft, H., 2016. Fused silica windows for solar receiver applications. In: Proc. SolarPACES 2015, AIP Conf. Proc. 1734, 030020.

Ho, C.K., Iverson, B.D., 2014. Review of high-temperature central receiver designs for concentrating solar power. Renew. Sustain. Energy Rev. 29, 835–846.

Hoffschmidt, B., 2014. Receivers for solar tower systems. < http://elib.dlr.de/94540/1/SFERA2014_SolarTowerReceivers_final.pdf > (28.08.17).

Hottel, H.C., Sarofim, A.F., 1967. Radiative Transfer. McGraw-Hill, New York.

IEA, 2016. Key world energy statistics. < https://www.iea.org/publications/freepublications/publication/KeyWorld2016.pdf > (28.08.17).

IEA-ESTAP, IRENA, 2015. Solar heat for industrial processes – technology brief. < http://www.irena.org/DocumentDownloads/Publications/IRENA_ETSAP_Tech_Brief_E21_Solar_Heat_Industrial_2015.pdf > (28.08.17).

Kangwanpongpan, T., França, F.H.R., da Silva, R.C., Schneider, P.S., Krautz, H.J., 2012. New correlations for the weighted-sum-of-gray-gases in oxy-fuel conditions based on HITEMP 2010 database. Int. J. Heat Mass Transf. 55, 7419–7433.

Khivsara, S.D., Srinivasan, V., Dutta, P., 2016. Radiative heating of supercritical carbon dioxide flowing through tubes. Appl. Therm. Eng. 109, 871–877.

Leckner, B., 1972. Spectral and total emissivity of water vapor and carbon dioxide. Combust. Flame 19, 33–48.

Modest, M.F., 1992. The Monte Carlo method applied to gases with spectral line structure. Numer. Heat Transf. B 22, 273–284.

Modest, M.F., 2013. Radiative heat transfer, 3rd ed. Academic Press, New York.

Naegler, T., Simon, S., Klein, M., Gils, H.C., 2015. Quantification of the European industrial heat demand by branch and temperature level. Int. J. Energy Res. 39, 2019–2030.

Patankar, S.V., 1980. Numerical Heat Transfer and Fluid Flow. Hemisphere, New York.

Philipp, H.R., 1998. Silicon dioxide (SiO2) glass. In: Palik, E.D. (Ed.), Handbook of Optical Constants of Solids, 3rd ed. Academic Press, New York.

Romero-Alvarez, M., Zarza, E., 2007. Concentrating solar thermal power. In: Kreith, F., Goswami, Y. (Eds.), Handbook of Energy Efficiency and Renewable Energy. CRC Press, Boca Raton.

Rothman, L.S., Gordon, I.E., Barber, R.J., Dothe, H., Gamache, R.R., Goldman, A., Perevalov, V.I., Tashkun, S.A., Tennyson, J., 2010. HITEMP, the high-temperature molecular spectroscopic database. J. Quant. Spectrosc. Radiat. Transf. 111, 2139–2150.

Siegel, R., Howell, J.R., 1992. Thermal Radiation Heat Transfer, 3rd ed. Hemisphere, New York.

Turchi, C.S., 2009. Supercritical CO2 for application in concentrating solar power systems. In: Proc. Supercritical CO2 Power Cycle Symposium, Rensselaer Polytechnic Institute, Troy.

Wang, A., Modest, M.F., 2007. Spectral Monte Carlo models for nongray radiation analyses in inhomogeneous participating media. Int. J. Heat Mass Transf. 50, 3877–3889.

Winston, R., Miñano, J.C., Benítez, P., Shatz, N.N., Bortz, J.C., 2005. Nonimaging Optics. Academic Press, New York.